Electric Vehicle Stability Control Based on Disturbance Accommodating Kalman Filter Using GPS

Binh Minh Nguyen[1], Yafei Wang[2], Hiroshi Fujimoto[1], Yoichi Hori[1]
[1]Department of Advanced Energy, the University of Tokyo, Japan
E-mail: minh@hori.k.u-tokyo.ac.jp, wang@hori.k.u-tokyo.ac.jp, fujimoto@k.u-tokyo.ac.jp, hori@k.u-tokyo.ac.jp

***Abstract*-This paper describes a new electronic stability control system of electric vehicles based on sideslip angle estimation through Kalman filter. Vehicle course angle obtained from single antenna GPS receiver and yaw rate obtained from gyroscope are used as measurements for Kalman filter. By treating the combination of model errors and external disturbances as extended states in the Kalman filter algorithm, accurate sideslip angle estimation was achieved. A new scheme was proposed for integrating active front steering angle and yaw moment as control inputs. The extended states are utilized for disturbance rejection that improves the robustness of the control system.**

***Keywords*-Sideslip angle, Kalman filter, electric vehicles, global positioning system, vehicle stability control**

I. INTRODUCTION

Electronic stability control (ESC) is one of the critical issues in motion control of EVs. In order to keep the vehicle moving on the intended path, both yaw rate and sideslip angle must be controlled to follow the reference values calculated from driver's inputs [1]. The following problems challenge the design of ESC system. The first is how to accurately obtain the sideslip angle. While yaw rate can be measured by popular gyroscope, sideslip angle sensors are very expensive for commercial vehicles. The second is how to design the control system as robust as possible. The ESC system of vehicle has to deal with the model uncertainties due the change of road conditions, and the influence of unknown disturbances such as lateral wind force.

Various methods of sideslip angle estimation have been proposed. Kinematic model based estimations do not rely on the tire force characteristics of vehicle [2], [3]. However these methods use accelerometers which drift over time due to sensor bias and strong noises presented in measurements. Moreover, the roll angle and road inclination introduce offset to lateral accelerometer because of the gravity. Although nonlinear dynamics model based estimations can be proof mathematically, these methods are complicated to implement in real time [4]. Using constant vehicle parameters (e.g., cornering stiffness) linear dynamics model based methods are not robust enough under the variation of road friction coefficient [5]. Online identification of tire cornering stiffness can be applied, but it will increase the computational burden of control system. Visual information can provide the heading angle of vehicle for sideslip angle estimation [6]. However, visual signals may be unavailable when road markers are covered with leaves, snow, water or dirt. In [7], the measurements of tire lateral forces enable sideslip angle identification without cornering stiffness. The high cost and the influence of strong noises are big hurdles in using tire lateral force sensors in vehicle motion control.

Since the last decade, global positioning system (GPS) has been a candidate for sideslip angle estimation. Using double antenna GPS receiver, sideslip angle could be calculated directly [8]. In [9], single antenna GPS receiver was combined with magnetometer for sideslip angle estimation. However, the use of double antenna receiver or single antenna receiver and magnetometer will increase the cost of control system. Due to the low update rate of GPS receiver (1-10 Hz), method proposed in [8] cannot satisfy advanced motion control of EVs which requires state estimation every 1 millisecond. By fusing the GPS receiver signal with the yaw rate sensor signal, sideslip angle can be estimated at high-rate [10]. However, the robustness of estimation under model uncertainties and external disturbances was not examined. Moreover, the problem of GPS measurement delay was not considered in [8] and [10]. The methods proposed in [8]-[10] have not been integrated with the lateral stability controller of EVs.

In [11], based on the principle of disturbance observer, lateral force observer and yaw moment observer were combined to improve the robustness of EVs' lateral stability control. However, this control system did not include a sideslip angle estimator.

In this paper, a new EVs' lateral stability control system based on Kalman filter using a single antenna GPS receiver is proposed. Following the idea of disturbance accommodating control [12], by treating the model uncertainties and external disturbances as extended states of Kalman filter, high accuracy of sideslip angle estimation is achieved. Active front steering and direct yaw moment generated by rear in-wheel motors are selected as control inputs for manipulating both sideslip angle and yaw rate. Instead of decoupling control, a new 2-DOF scheme is proposed for lateral stability control design. The extended states are used for disturbance rejection that improves the robustness of the system. Experimented and simulations were conducted to verify the effectiveness of the proposed algorithms.

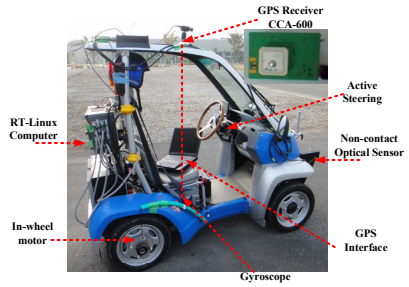

Fig. 1. Experimental electric vehicle and GPS receiver.

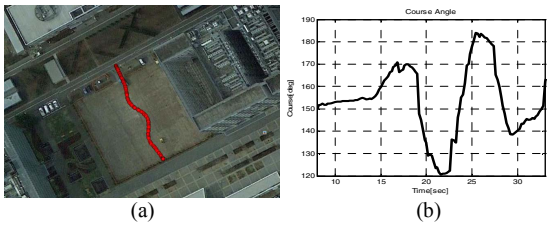

(a) (b)

Fig. 2. Data obtained by GPS software.
(a) Position on Google Earth. (b) Course angle.

TABLE I
NOMENCLATURES

l_f, l_r	Distances from front and rear axle to CG
C_f, C_r	Front and rear cornering stiffness
I_z	Yaw moment of inertia
δ_f	Front steering angle
N_z	Yaw moment
M	Vehicle mass
β	Sideslip angle
γ	Yaw rate
ψ	Yaw angle
c	Course angle obtained from GPS
v_x	Longitudinal velocity

II. EXPERIMENT SYSTEM

To verify the effectiveness of the proposed algorithms, a micro in-wheel motored EV name "super-capacitor COMS" was used (Fig. 1). Two in-wheel motors are placed in the rear-left and rear-right wheels. Active front steering is used as another actuator of the control system. It enables the steer-by-wire mode. A noncontact optical sensor (produced by Corrsys-Datron) is used for accurate acquisition of sideslip angle. Estimation and control algorithms were implemented in RT-Linux computer which is the center of the control system. GPS receiver CCA-600 produced by Japan Radio Co. Ltd. was used in this study. It can provide the course angle measurement with the accuracy of 0.14 degree RMS at the vehicle velocity of 60 kph. Course angle is the angle between the vehicle velocity vector and the geodetic North. Vehicle position and course angle obtained through a lane-change test are shown in Fig. 2.

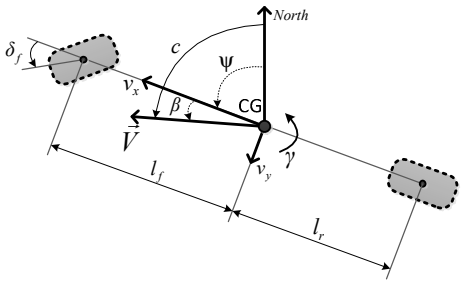

Fig. 3. Planar bicycle model of electric vehicle.

III. VEHICLE MODELING

The linear bicycle model shown in Fig. 3 was constructed under the following assumptions: 1) Tire slip angle is small so that the lateral component of tire force is at linear region. 2) Vehicle is symmetric about the fore-and-aft center line. 3) Load transfer, roll motion, and pitch motion are neglected.

The influence of external disturbances to the vehicle system can be generalized as the lateral force disturbance F_d and yaw moment disturbance N_d. To demonstrate the motion of vehicle, the lateral force equation and the yaw moment equation are derived as follows:

$$Mv_x\left(\dot{\beta}+\gamma\right)=-2C_f\left(\beta+\frac{l_f\gamma}{v_x}-\delta_f\right)-2C_r\left(\beta-\frac{l_r\gamma}{v_x}\right)+F_d \tag{1}$$

$$I_z\dot{\gamma}=-2C_f\left(\beta+\frac{l_f\gamma}{v_x}-\delta_f\right)l_f+2C_r\left(\beta-\frac{l_r\gamma}{v_x}\right)l_r+N_z+N_d \tag{2}$$

Course angle is represented as the summary of yaw angle and sideslip angle:

$$c=\psi+\beta \tag{3}$$

IV. SIDESLIP ANGLE ESTIMATION DESIGN

A. Disturbance Accommodating Dynamics Model

The estimation model is designed using the nominal cornering stiffness C_{fn} and C_{rn}. Due to the change of road conditions, the true cornering stiffness differ from the nominal values. The variation of tire cornering stiffness can be expressed as follows:

$$C_f=C_{fn}+\Delta C_f,\ C_r=C_{rn}+\Delta C_r \tag{4}$$

From (1)-(4), lateral dynamics model is derived as follows:

$$\dot{x}=A_n x+B_n u+D_n\varsigma+w \tag{5}$$

$$x=\begin{bmatrix}\beta & \gamma & \psi\end{bmatrix}^T,\ u=\begin{bmatrix}\delta_f & N_z\end{bmatrix}^T,\ \varsigma=\begin{bmatrix}d_1 & d_2\end{bmatrix}^T \tag{6}$$

$$A_n=\begin{bmatrix}a_{n11} & a_{n12} & 0\\ a_{n21} & a_{n22} & 0\\ 0 & 1 & 0\end{bmatrix},\ B_n=\begin{bmatrix}b_{n11} & b_{n12}\\ b_{n21} & b_{n22}\\ 0 & 0\end{bmatrix},\ D_n=\begin{bmatrix}1 & 0\\ 0 & 1\\ 0 & 0\end{bmatrix} \tag{7}$$

$$d_1=\frac{-2\left(\Delta C_f+\Delta C_r\right)}{Mv_x}\beta+\frac{-2\left(\Delta C_f l_f-\Delta C_r l_r\right)}{Mv_x^2}\gamma+\frac{2\Delta C_f}{Mv_x}\delta_f+\frac{1}{Mv_x}F_d \tag{8}$$

$$d_2 = \frac{-2\left(\Delta C_f l_f - \Delta C_r l_r\right)}{I_z}\beta + \frac{-2\left(\Delta C_f l_f^2 + \Delta C_r l_r^2\right)}{I_z v_x}\gamma + \frac{2\Delta C_f l_f}{I_z}\delta_f + \frac{1}{I_z}N_d \tag{9}$$

$$\begin{bmatrix} a_{n11} & a_{n12} \\ a_{n21} & a_{n22} \end{bmatrix} = \begin{bmatrix} \frac{-2\left(C_{fn}+C_{rn}\right)}{Mv_x} & -1-\frac{2\left(C_{fn}l_f - C_{rn}l_r\right)}{Mv_x^2} \\ \frac{-2\left(C_{fn}l_f - C_{rn}l_r\right)}{I_z} & \frac{-2\left(C_{fn}l_f^2 + C_{rn}l_r^2\right)}{I_z v_x} \end{bmatrix} \tag{10}$$

$$\begin{bmatrix} b_{n11} & b_{n12} \\ b_{n21} & b_{n22} \end{bmatrix} = \begin{bmatrix} \frac{2C_{fn}}{Mv_x} & 0 \\ \frac{2C_{fn}l_f}{I_z} & \frac{1}{I_z} \end{bmatrix} \tag{11}$$

In this paper, it is assumed that the model uncertainties mainly rely on tire cornering stiffness variation. In the above dynamics equations, d_1 and d_2 are the unknown disturbance terms which represent the influences of cornering stiffness variation and external disturbances, and w is the process noise vector. The continuous time model (5) is transformed to the discrete time model (12) using the transformation (13). T_c is the fundamental sampling time which is 1 millisecond.

$$x_{k+1} = A_{nd}x_k + B_{nd}u_k + D_{nd}\varsigma_k + w_k \tag{12}$$

$$A_{nd} = e^{A_n T_c},\ B_{nd} = \int_0^{T_c} e^{A_n \tau} d\tau B_n,\ D_{nd} = \int_0^{T_c} e^{A_n \tau} d\tau D_n \tag{13}$$

In [12], disturbance accommodating control was firstly introduced. The key idea is that the external disturbances can be augmented to be the extended states of the system. Assuming that the disturbance terms are stochastic processes with zero-mean white noise sequence as in (14), a new state space model is constructed as (15)-(17).

$$\varsigma_{k+1} = \varsigma_k + w_{dis,k} \tag{14}$$

$$X_{k+1} = \tilde{A}_{nd}X_k + \tilde{B}_{nd}U_k + W_k \tag{15}$$

$$X_k = \begin{bmatrix} x_k \\ \varsigma_k \end{bmatrix},\ U_k = u_k,\ W_k = \begin{bmatrix} w_k \\ w_{dis,k} \end{bmatrix} \tag{16}$$

$$\tilde{A}_{nd} = \begin{bmatrix} A_{nd} & D_{nd} \\ [0]_{2\times 3} & [I]_{2\times 2} \end{bmatrix},\ \tilde{B}_{nd} = \begin{bmatrix} B_{nd} \\ [0]_{2\times 2} \end{bmatrix} \tag{17}$$

where $[I]$ represents the unity matrix, $[0]$ represents the zero matrix, and W_k is the process noise vector of the disturbance accommodating system at step k.

B. Multi-rate Measurements

In this paper, the yaw rate and the course angle are selected as measurements. While the yaw rate's sampling time is T_c = 1 millisecond, the sampling time of course angle obtained from GPS is much longer. For fair comparison with the works in [8]-[10], 5 Hz update mode was set for the receiver CCA-600. This yields the course angle sampling time of T_s = 200 milliseconds. From (3), the measurement equation is expressed as follows:

$$Y_k = \tilde{C}_{nd}X_k + V_k \tag{18}$$

If course angle is updated (k = T_s/T_c):

$$\tilde{C}_{nd} = \begin{bmatrix} 0 & 1 & 0 & 0 & 0 \\ 1 & 0 & 1 & 0 & 0 \end{bmatrix} \tag{19}$$

If course angle is not updated (k ≠ T_s/T_c):

$$\tilde{C}_{nd} = \begin{bmatrix} 0 & 1 & 0 & 0 & 0 \\ 0 & 0 & 0 & 0 & 0 \end{bmatrix} \tag{20}$$

where V_k is the measurement noise vector at step k.

C. Noise Covariance Matrices

Q_W and R_V are process noise and measurement noise covariance matrices. Q_W represents the accuracy of dynamics model and R_V shows the level of confidence placed in sensor measurements. In order to reduce the computational time when implementing the algorithm in real-time control system, Q_W and R_V are treated as diagonal matrices:

$$Q_W = \mathrm{diag}\left[Q_\beta, Q_\gamma, Q_\psi, Q_{d_1}, Q_{d_2}\right] \tag{21}$$

$$R_V = \mathrm{diag}\left[R_\gamma, R_c\right] \tag{22}$$

In this paper, trial-and-error method was conducted to select the suitable noise covariance matrices. Auto-tuning of noise covariance matrices will be examined in future works.

D. Kalman Filter Algorithms

The disturbance accommodating Kalman filter (DAKF) algorithm shown in Fig. 4 includes two stages: 1) Prediction based on the disturbance accommodating dynamics model. 2) Correction based on multi-rate measurements.

The observability of sideslip angle and disturbance terms are assured by checking the rank of matrix $\left[\tilde{C}_{nd} \quad \tilde{C}_{nd}\tilde{A}_{nd} \quad \cdots \quad \tilde{C}_{nd}\tilde{A}_{nd}^4\right]^T$ .Using the proposed algorithm, even if the GPS based measurement is unavailable (e.g., the number of satellites in view is smaller than 4), sideslip angle can be estimated using only yaw rate.

V. LATERAL STABILITY CONTROL DESIGN

A. Reference Model for Lateral Motion

The reference model is determined based on the steady state response of sideslip angle and yaw rate in respect of the steering command given by the driver. From (1) and (2), the reference values can be calculated as follows:

$$\beta_d = \frac{1-\frac{M}{2\left(l_f+l_r\right)}\frac{l_f}{C_{rn}l_r}v_x^2}{1+Gv_x^2}\frac{l_r}{\left(l_f+l_r\right)}\delta_{cmd},\ \gamma_d = \frac{1}{1+Gv_x^2}\frac{v_x}{\left(l_f+l_r\right)}\delta_{cmd} \tag{23}$$

$$G = \frac{M}{2\left(l_f+l_r\right)^2}\frac{C_{rn}l_r - C_{fn}l_f}{C_{fn}C_{rn}} \tag{24}$$

B. Design of Disturbance Rejection

The dynamics of the lateral motion can be expressed in state space form:

$$\begin{bmatrix} \dot{\beta} \\ \dot{\gamma} \end{bmatrix} = \begin{bmatrix} a_{n11} & a_{n12} \\ a_{n21} & a_{n22} \end{bmatrix}\begin{bmatrix} \beta \\ \gamma \end{bmatrix} + \begin{bmatrix} b_{n11} & b_{n12} \\ b_{n21} & b_{n22} \end{bmatrix}\begin{bmatrix} \delta_f \\ N_z \end{bmatrix} + \begin{bmatrix} d_1 \\ d_2 \end{bmatrix} \tag{25}$$

To compensate the influence of disturbances, the disturbance matrix is designed as follows:

$$C_{dis}=\begin{bmatrix} b_{n11} & b_{n12} \\ b_{n21} & b_{n22} \end{bmatrix}^{-1} \tag{26}$$

With the disturbance rejection, the system is augmented to be the nominal model. Therefore, the feed-back and feed-forward controller were designed using the nominal model.

C. Design of Feed-forward Controller

From (25), the nominal transfer function P_n from the control input vector to the controlled state vector is derived as (27). The feed-forward controller is designed as the inverse matrix of P_n, given by (28). I is the unity matrix.

$$P_n=\left(sI-\begin{bmatrix} a_{n11} & a_{n12} \\ a_{n21} & a_{n22} \end{bmatrix}\right)^{-1}\begin{bmatrix} b_{n11} & b_{n12} \\ b_{n21} & b_{n22} \end{bmatrix} \tag{27}$$

$$C_{ff}=P_n^{-1}=\begin{bmatrix} C_{ff11} & C_{ff12} \\ C_{ff21} & C_{ff22} \end{bmatrix} \tag{28}$$

$$\begin{aligned} C_{ff11}&=\frac{(b_{n22}s-b_{n22}a_{n11})}{b_{n11}b_{n22}}, C_{ff12}=\frac{-a_{n12}}{b_{n11}} \\ C_{fb21}&=\frac{(-b_{n21}s-b_{n11}a_{n21}+b_{n21}a_{n11})}{b_{n11}b_{n22}}, C_{ff22}=\frac{(b_{n11}s+b_{n21}a_{n12}-b_{n11}a_{n22})}{b_{n11}b_{n22}} \end{aligned} \tag{29}$$

D. Design of Feed-back Controller

The desired transfer function matrix of the closed loop system including the feed-back controller and the plant is selected as follows:

$$K=\mathrm{diag}\left[\frac{K_\beta}{s+K_\beta},\frac{K_\gamma}{s+K_\gamma}\right] \tag{30}$$

In (30), if the cut-off frequency K_β and K_γ are low, the responses of sideslip angle and yaw rate are too slow to track the desired values. On the other hand, it is impossible to set the cut-off frequencies too high due to the limitation of the actuators and the stability of the control system including the Kalman filter. In this study, by conducting experiments, K_β and K_γ are chosen as 5 rad/s. The feedback controller is designed by the model following method:

$$\begin{aligned} &\left(I+P_nC_{fb}\right)^{-1}P_nC_{fb}=K \\ &\Rightarrow C_{fb}=P_n^{-1}K\left(I-K\right)^{-1}=\begin{bmatrix} C_{fb11} & C_{fb12} \\ C_{fb21} & C_{fb22} \end{bmatrix} \end{aligned} \tag{31}$$

$$\begin{aligned} C_{fb11}&=\frac{(b_{n22}s-b_{n22}a_{n11})(s+K_\gamma)}{b_{n11}b_{n22}s}\frac{K_\beta}{s+K_\beta} \\ C_{fb12}&=\frac{-a_{n12}(s+K_\beta)}{b_{n11}s}\frac{K_\gamma}{s+K_\gamma} \\ C_{fb21}&=\frac{(-b_{n21}s-b_{n11}a_{n21}+b_{n21}a_{n11})(s+K_\gamma)}{b_{n11}b_{n22}s}\frac{K_\beta}{s+K_\beta} \\ C_{fb22}&=\frac{(b_{n11}s+b_{n21}a_{n12}-b_{n11}a_{n22})(s+K_\beta)}{b_{n11}b_{n22}s}\frac{K_\gamma}{s+K_\gamma} \end{aligned} \tag{32}$$

The feed-back controller augmented the closed loop system to the desired model K with the poles placed at $-K_\beta$ and $-K_\gamma$. The internal stability of the closed loop system is assured by verifying the poles of the following matrices of transfer function:

$$P_n^{-1}\left(I+P_nC_{fb}\right)^{-1}P_nC_{fb} \text{ and } \left(P_nC_{fb}\right)^{-1}\left(I+P_nC_{fb}\right)^{-1}P_nC_{fb}$$

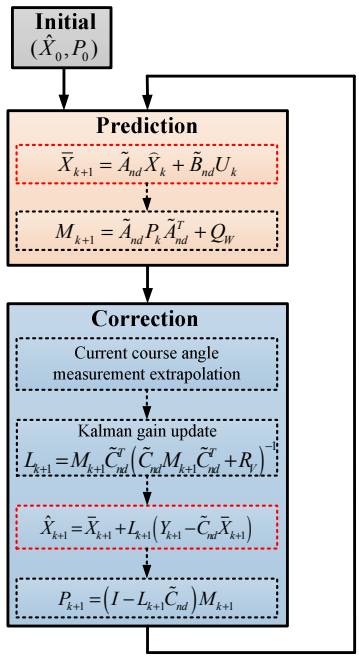

Fig. 4. Kalman filter algorithm.

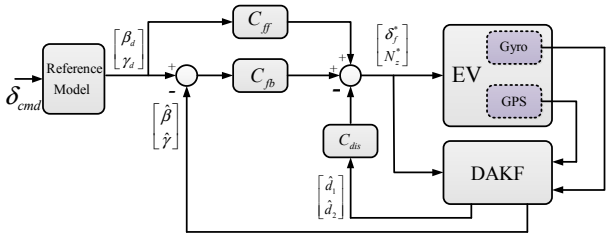

Fig. 5. Lateral stability control system of electric vehicle.

E. Front Steering and Yaw Moment Commands

The general lateral stability control system of electric vehicle is shown in Fig. 5. The commands outputted from the controller are obtained as follows:

$$\begin{bmatrix} \delta_f^* \\ N_z^* \end{bmatrix}=C_{fb}\begin{bmatrix} \beta_d-\hat{\beta} \\ \gamma_d-\hat{\gamma} \end{bmatrix}+C_{ff}\begin{bmatrix} \beta_d \\ \gamma_d \end{bmatrix}-C_{dis}\begin{bmatrix} \hat{d}_1 \\ \hat{d}_2 \end{bmatrix} \tag{33}$$

The feed-forward controller contains improper transfer functions. However, feed-forward commands are realizable because the derivative of the reference values can be calculated. From the yaw moment and acceleration commands, the torque commands distributed to the rear-left and rear-right in wheel motors are derived. An EPS motor is used for tracking the real front steering angle with the steering command.

VI. SIMULATION RESULTS

A. Simulation of Sideslip Angle Estimation

Using Matlab/Simulink, simulations were conducted to verify the proposed DAKF. Other two methods were also performed for comparing. The first is sideslip angle estimation using linear observer (LOB) with constant

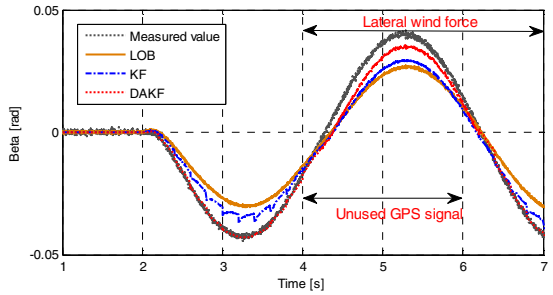

(a)

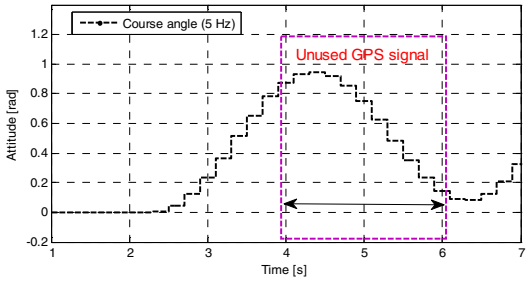

(b)

Fig. 6. Simulation results of sideslip angle estimation. (a) Sideslip angle. (b) Course angle.

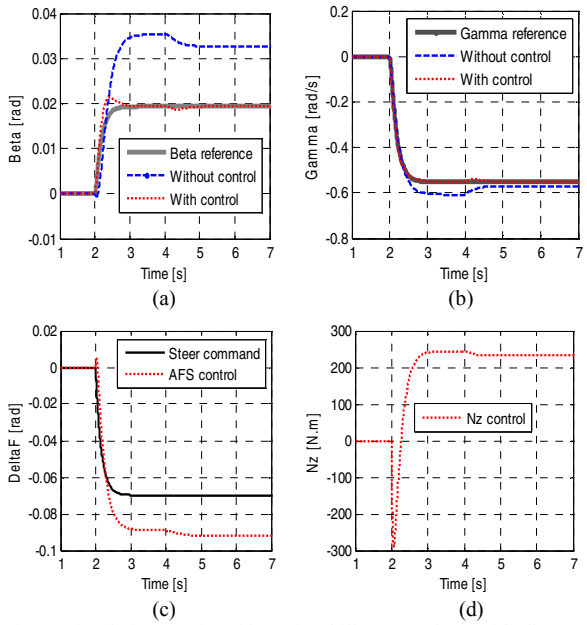

(a) (b) (c) (d)

Fig. 7. Simulation results of lateral stability control. (a) Sideslip angle. (b) Yaw rate. c) Front steering angle. d) Yaw moment command

cornering stiffness model [5]. This method uses lateral acceleration and yaw rate as measurements. The second is the Kalman filter (KF) with the measurements of GPS course angle and yaw rate [10]. A case of simulation test is demonstrated in this paper, the lane-change test with sinusoidal steering command, as shown in Fig. 6. The following conditions were set: 1) Velocity is 25 kph. 2) Lateral wind force influences the system from 4 to 8 seconds. 3) GPS signal is unavailable from 4 to 6 second. 4) The cornering stiffness of the vehicle model: $C_f = C_r = 7000$ N/rad. However, a big variation is introduced to the estimation model's cornering stiffness: $C_{fn} = C_{rn} = 10{,}000$ N/rad. 5) Fundamental sampling time is 1 millisecond and course angle measurement is sampled at 200 milliseconds. The simulation results show that: LOB has the poorest sideslip angle estimation performance. Using course angle from GPS, KF has the better performance than LOB. However, this method is still sensitive to the influence of model error and lateral wind force. The proposed DAKF shows the smaller estimation error in comparison with that of LOB and KF. From 4.0 to 6.0 second, even if GPS signal is unused, DAKF has smaller estimation error than KF and LOB. After 6 second, GPS signal is recovery, the estimated sideslip angle by DAKF continues to track with the true value.

B. Simulation of Lateral Stability Control

After evaluating the estimation algorithm, the Matlab/Simulink model of the whole system in Fig. 5 was constructed. This model simulates the steer-by-wire mode such that the steering command is generated by program and the front steering angle is generated by only the EPS motor. Model error and lateral wind force were set as the previous simulations. Fig. 7 shows the results of simulation tests with step steer command. Without the proposed control system, both the yaw rate and sideslip angle increase above the reference values. In contrast, with the proposed control system, active front steering and yaw moment are generated to assure the tracking of the yaw rate and the sideslip angle.

VII. EXPERIMENTAL RESULTS

A. Experiments of Sideslip Angle Estimation

The estimation algorithms were implemented in the experimental vehicle using C programming. Experiment condition is set as follows: 1) The tire cornering stiffness are approximately $C_f = C_r \approx 7000$ N/rad while the nominal cornering stiffness of estimation model are set as $C_{fn} = C_{rn} = 10{,}000$ N/rad. 2) Velocity of vehicle is controlled at about 20 kph. 3) To simulate the lost of GPS signal, course angle measurement is intentionally unused from 10.5 to 13.0 second. 4) Steering command is generated by the driver. Estimation results of lane-change test are demonstrated in this section. As shown in Fig. 8, LOB has biggest estimation error. KF is better than LOB, but still sensitive to model uncertainties. On the other hand, the estimated sideslip angle by DAKF can track with the measured value obtained from the optical sensor. The simulation and experiment show that the used of disturbance accommodating and GPS can improve the robustness of sideslip angle estimation. From 10.5 to 13.0 second, even if the course angle measurement is unused, DAKF shows the smaller estimation error than that of LOB and KF, thanks to the disturbance estimation.

B. Experiments of Lateral Stability Control

The results of cornering test are shown in Fig. 9. Instead of handling by the driver, steer-by-wire mode was used for generating front steering angle. The steering command was pre-designed and generated by the program. The vehicle velocity was controlled at about 20 kph. By this way, the

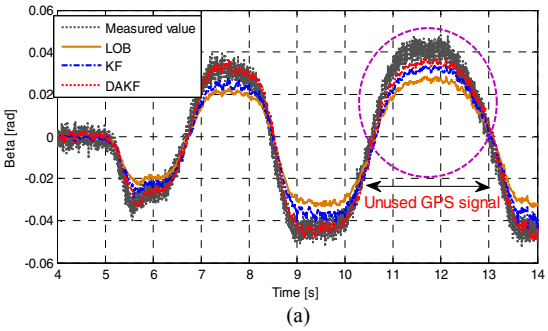

(a)

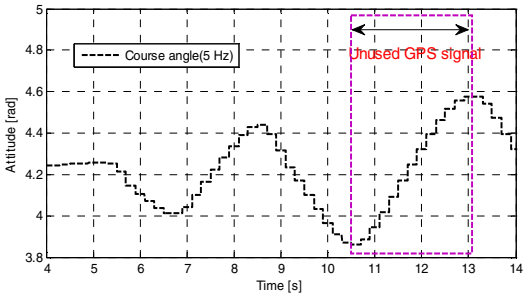

(b)

Fig. 8. Experiment results of sideslip angle estimation. (a) Sideslip angle. (b) Course angle.

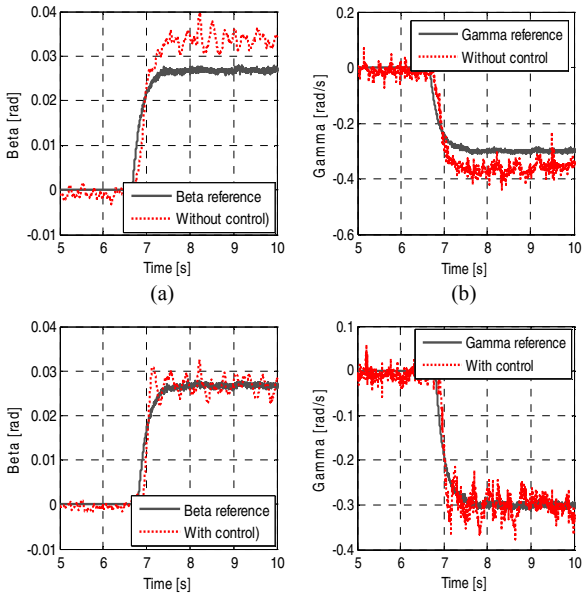

(a) (b) (c) (d)

Fig. 9. Experimental results of lateral stability control. (a) Sideslip angle: *without control*. (b) Yaw rate: *without control*. c) Sideslip angle: *with control*. d) Yaw rate: *with control*

same driving condition was made for the cases of with stability control and without stability control. The cornering stiffness error was set as the above estimation experiments. In case of without control, the response of sideslip angle and yaw rate could not track with the reference values. When the proposed control system was applied, the tracking control was successfully performed. This shows the improvement of the stability of the vehicle motion.

VIII. CONCLUSIONS

This paper proposes the disturbance accommodating Kalman filter (DAKF) using GPS for electronic stability control system of in-wheel motored EVs. In the algorithm, the delay of course angle obtained from GPS was handled. Simulations and experiments show that the proposed algorithm can improve the robustness of sideslip angle estimation under the influence of model errors and external disturbances. Even if the GPS signal is unavailable, sideslip angle can be estimated. Based on the DAKF and the integration of active front steering and yaw moment, a new scheme for EV's lateral stability control was designed. Besides state estimation, DAKF enables disturbance estimation and rejection that improve the robustness of the control system. Future works concern the following problems: 1) How to tune the noise covariance according to GPS measurement in real time. 2) How to improve the estimation between two consecutive updates of GPS measurement.

REFERENCES

[1] J. Y. Wong, "Theory of Ground Vehicles," John Wiley & Sons, INC, Third Edition, 2001.

[2] B. C. Chen, F. C. Hsieh, "Sideslip Angle Estimation Using Extended Kalman Filter," *Vehicle System Dynamics*, Vol. 46, No. 1, pp. 353-364, 2008.

[3] M. Corno, M. Tanelli, A. Zappavigna, S. M. Savaresi, A. Fortina, and S. Campo, "Designing On-Demand Four-Wheen-Drive Vehicles via Active Control of the Central Transfer Case," *IEEE Transactions on Intelligent Transportation Systems*, Vol. 11, No. 4, pp. 931-941, 2010.

[4] L. Imsland, T. A. Johansen, T. I. Fossen, H. F. Grip, J. C. Kalkkuhl, and A. Suissa, "Vehicle Velocity Estimation Using Nonlinear Observers," *Automatica*, Vol. 42, No. 12, pp. 2091-2103, 2006.

[5] Y. Aoki, T. Inoue, and Y. Hori, "Robust Design of Gain Matrix of Body Slip Angle Observer for Electric Vehicles and Its Experimental Demonstration," 8th IEEE International Workshop on Advanced Motion Control, pp. 41-45, 2004.

[6] Y. Wang, B. M. Nguyen, P. Kotchapansompote, H. Fujimoto, and Y. Hori, "Image-Processing-Based State Estimation for Lateral Control of Electric Vehicle Using Multi-Rate Kalman Filter," *Recent Patents on Signal Processing*, Vol. 2, No. 2, pp. 140-148, 2012.

[7] K. Nam, H. Fujimoto, and Y. Hori, "Lateral Stability Control of In-Wheel-Motor-Driven Electric Vehicles Based on Sideslip Angle Estimation Using Lateral Tire Force Sensors," IEEE Transactions on Vehicular Technology, Vol. 61, No. 5, pp. 1972-1985, 2012.

[8] D. M. Bevly, J. Ryu, and J. C. Gerdes, "Integrating INS Sensors With GPS Measurements for Continuous Estimation of Vehicle Sideslip, Roll, and Tire Cornering Stiffness," *IEEE Transactions on Intelligent Transportation System*, Vol. 7, No. 4, pp. 483-493, 2006.

[9] J. H. Yoon and H. Peng, "Sideslip Angle Estimation Based on GPS and Magnetometer Measurements," *Proceeding of 11th International Symposium on Advanced Vehicle Control* (AVEC), Korea, 2012.

[10] R. Anderson and D. M. Bevly, "Using GPS with a Model-Based Estimator to Estimate Critical Vehicle States," *Vehicle System Dynamics*, Vo. 48, No. 12, pp. 1413-1438, 2010.

[11] H. Fujimoto and Y. Yamauchi, "Advanced Motion Control of Electric Vehicle Based on Lateral Force Observer with Active Steering," *Proceeding of 2010 IEEE International Symposium on Industrial Electronics* (ISIE), pp. 3627-3632, 2010.

[12] C. Johnson, "Accommodation of External Disturbances in Linear Regulator and Servomechanism Problem," *IEEE Transaction on Automatic Control*, Vol. 16, No. 6, pp. 535-644, 1971.